IOPscience iopscience.iop.org

Home Search Collections Journals About Contact us My IOPscience

Laser direct writing of modulation-doped nanowire p/n junctions

This content has been downloaded from IOPscience. Please scroll down to see the full text.

2016 Nanotechnology 27 485205

(http://iopscience.iop.org/0957-4484/27/48/485205)

View the table of contents for this issue, or go to the journal homepage for more

Download details:

IP Address: 128.46.222.252
This content was downloaded on 04/11/2016 at 14:37

Please note that terms and conditions apply.

Nanotechnology **27** (2016) 485205 (5pp) doi:10.1088/0957-4484/27/48/485205

Laser direct writing of modulation-doped nanowire p/n junctions

Woongsik Nam[1,2], **James I Mitchell**[1,2,3] and **Xianfan Xu**[1,2]

[1] School of Mechanical Engineering, Purdue University, West Lafayette, IN 47907, USA
[2] Birck Nanotechnology Center, Purdue University, West Lafayette, IN 47907, USA

E-mail: xxu@ecn.purdue.edu

Received 25 August 2016, revised 4 October 2016
Accepted for publication 14 October 2016
Published 4 November 2016

Abstract

We demonstrate a single-step, laser-based technique to fabricate axial modulation-doped silicon nanowires. Our method is based on laser-direct-write chemical vapor deposition and has the capability to fabricate nanowires as small as 60 nm, which is far below the diffraction limit of the laser wavelength of 395 nm, with precise control of nanowire position, length, and orientation. By switching dopant gases during nanowire writing, p–n junction nanowires are produced. The p–n junction nanowires are fabricated into multifinger devices with parallel metal contacts and electrically tested to demonstrate diode characteristics.

Keywords: nanowire, p/n junction, laser synthesis

(Some figures may appear in colour only in the online journal)

1. Introduction

Growing silicon nanowires (SiNWs) using the vapor–liquid–solid (VLS) mechanism has attracted significant attentions due to their potential for high-performance nanoscale devices [1, 2]. The VLS method can also be used to modulate dopant profiles in nanowires to create devices such as diodes [3], photovoltaics [4], and tunnel field-effect transistors [5]. Although VLS-grown nanowires have advantages of crystallinity, small diameters, and *in situ* doping, the difficulty in precisely controlling the position and orientation of nanowires has been a major obstacle to creating large arrays of nanowires. Undesirable metal contamination due to metal catalysts during nanowire growth is another drawback [6]. When forming longitudinal modulation-doped nanowires, the radial deposition after changing growth conditions has also been a concern [7, 8].

Laser heating has long been combined with chemical vapor deposition (CVD) for materials deposition [9, 10]. Laser-based material deposition schemes are highly flexible and compatible with *in situ* doping, but wider uses for micro and nanoscale devices were inhibited by scaling limitations due to the diffraction limit. On the other hand, direct writing of laser induced periodic surface structures (LIPSS) has been an area of ongoing examination to form features well below the processing wavelength in nearly all types of materials [11, 12]. Significant progress has been made to understand the principles behind LIPSS formation [12–14], to improve their manufacturability [15], and to use LIPSS for bulk surface texturing for enhancing or altering material absorptivity [16, 17]. One way to open LIPSS up to more applications is to expand from the predominant focus on material removal, and to instead apply them to material growth. Incorporating LIPSS into direct writing of doped CVD films gives the potential to transition the diffraction-limited, laser-based materials growth techniques down into the nanometer regime with intricate dopant profiles.

A recently developed method utilizes lasers to directly write nanowires by laser-induced CVD [18]. It was shown that this method is capable of producing sub-diffraction limited nanowires, as small as 60 nm based on LIPSS [18]. The method relies on local heating without the use of metal catalysts, and therefore it readily lends itself to fabricating modulation-doped materials without concerns of additional deposition in other areas or metal contamination, and with the high level of placement control. In addition, the method has the potential to produce more functional nanowire morphology which can be similar to zigzag nanowires demonstrated in [19]. Since the nanowire forms parallel to the electric field polarization direction of the laser, the method has the

[3] Currently with Maxim Integrated, Beaverton, OR 97005, USA.

 © 2016 IOP Publishing Ltd Printed in the UK

potential to create kinked nanowires by changing the polarization direction and the nanowire writing direction simultaneously. Multiple nanowires can be simultaneously produced in one laser spot by adjusting the laser power [18].

In this work, we demonstrate a single-step, laser-direct-write CVD technique to form axial modulation-doped SiNWs. By combining the laser-direct-write CVD, the sub-diffraction feature sizes of LIPSS, and *in situ* doping, our method overcomes scaling limitations of traditional laser-based CVD, resulting in doped nanowires with diameters as small as 60 nm. P–n junction nanowires are synthesized by switching dopant gases during nanowire deposition. The p–n junction nanowires are electrically characterized to demonstrate the successful fabrication of the p–n transition. Kelvin probe force microscopy (KPFM) is used to provide the transition characteristics of the nanowires.

2. Experimental details

Nanowires were grown by laser heating the substrate surface which raised the temperature locally and decomposed the chemical gases. The substrate was translated during growth to create the feature patterns. Laser illumination was provided by a frequency doubled Ti:Sapphire femtosecond laser with a wavelength of 395 nm. The laser was focused on the substrate surface using Fresnel phase zone plates with a numerical aperture of 0.95. The pulse length measured using an autocorrelator before frequency doubling was 38 fs, and typical powers used to grow individual nanowires were between 6 and 10 mW. The substrates used for nanowire growth were 200 nm of top layer silicon dioxide, with an underlying 200 nm polysilicon layer all on 1 mm thick quartz. The top layer of silicon dioxide provides electrical insulation for nanowire devices, while the polysilicon layer serves to completely absorb the laser energy. The process gases were delivered to the laser focused area on the substrate through a flexible metal nozzle which is positioned very close to the substrate. Details of the laser CVD growth of nanowires have been described previously [18]. To produce nanowires with modulation doping, the growth chamber pressure was maintained at 2 Torr with a flow rate of 10 sccm of 10% silane balanced in argon. 500 ppm diborane (B_2H_6) in hydrogen with a flow rate of 1 sccm was used for p-type doping, and 100 ppm phosphine (PH_3) in hydrogen with a flow rate of 1 sccm for n-type doping. Using the flow rates of SiH_4, B_2H_6, and PH_3, the concentration ratios of SiH_4:B_2H_6 and SiH_4:PH_3 were calculated to be 2000:1 and 10 000:1, respectively. The nanowire growth started with one type of dopant and then the dopant was switched to the opposite polarity during the nanowire growth for p–n junction nanowires. The speed of the nanowire deposition was 0.5 μm s^{-1}.

A scanning electron microscopy image of a p–n junction SiNW is shown in figure 1(a). The nanowire forms parallel to the direction of laser polarization and the diameter of the nanowire is about 60 nm, far below the diffraction limit of the laser wavelength of 395 nm. The transition region between dopant polarities is near the middle of the nanowire in figure 1(a) and no change in nanowire diameter or shape is observed across the p–n transition. It is also seen that the nanowire is not perfectly straight, due to the instability of the piezoelectric stage that translates the substrate during the nanowire growth. The as-deposited nanowires were amorphous silicon [19].

Once p–n junction nanowires were synthesized, multifinger devices were fabricated to electrically characterize the nanowires. The multifinger devices had parallel metal contacts spaced by 5 μm gaps spanning the nanowires as shown in figure 1(b) and every two adjacent metal contacts formed a two-terminal device. The fabrication started with annealing the nanowires at 800 °C for 6 h to crystallize the amorphous silicon into polycrystalline silicon [19]. Ni contact pads were then deposited using electron beam lithography and electron beam evaporation. The devices were finally annealed at 350 °C for 1 min in forming gas (4% H_2/96% N_2) to form nickel silicide at the Ni–Si interfaces. In figure 1(b), the section in the middle of the nanowire includes a p–n junction and the left and right sides of the nanowire are p-type and n-type silicon, respectively. Electrical characteristics of the nanowire devices were measured in dark condition using a Keithley 4200-SCS semiconductor parameter analyzer. A Combiscope 1000 atomic force microscope (AFM) system (AIST-NT Inc.) and Pt/Ir-coated Si cantilevers with a spring constant of 42 N m^{-1} were used for the KPFM measurement.

3. Results and discussion

Since the post-growth annealing at 800 °C will cause lateral diffusion of dopant atoms, the diffusion lengths of boron and phosphorus in silicon during annealing were estimated. According to Fair's vacancy model, the diffusion coefficient of impurities in silicon can be calculated using the following equation [20]:

$$D = D^0 + \frac{n}{n_i}D^- + \left[\frac{n}{n_i}\right]^2 D^{2-} + \frac{p}{n_i}D^+ + \left[\frac{p}{n_i}\right]^2 D^{2+}, \quad (1)$$

where D^0, D^-, D^{2-}, D^+ and D^{2+} are the neutral, negative vacancy one, negative vacancy two, positive vacancy one, and positive vacancy two diffusivities, respectively, n_i is the intrinsic carrier concentration, and n and p are the electron and hole concentrations. Assuming for the sake of simplicity that the SiNWs are single crystalline, the characteristic diffusion length, $\sqrt{Dt}$, is calculated to be 22 nm for boron and 7.6 nm for phosphorus. Since the impurity diffusivity can be several times higher in polycrystalline silicon than in single-crystalline silicon [21], the actual diffusion lengths in our nanowires can be a few times higher than the calculated values. On the other hand, the calculated diffusion lengths are yet much smaller than the measured transition length of 1.5 μm which will be discussed later, therefore, we believe that the annealing process had limited effect on the transition length of the p–n junctions in the nanowires.

Figure 2 shows the electrical measurement results across each nanowire section. The p–n junction section demonstrates

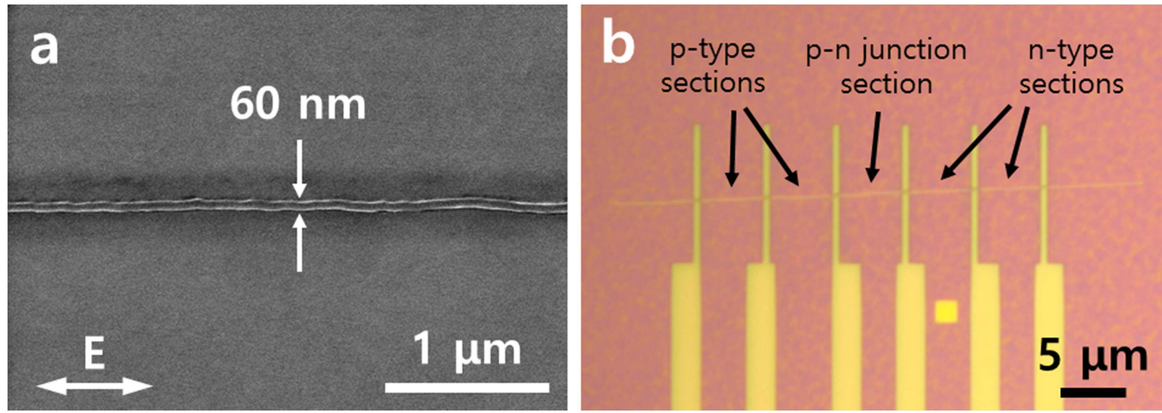

Figure 1. (a) SEM image of a laser-direct-written p–n junction Si nanowire. The white arrow indicates the electric field polarization direction of the incident laser. (b) Optical image of a multifinger device fabricated from a p–n junction nanowire.

the expected diode behavior as seen in figure 2(a). When positive voltages are applied to the p-side terminal, increased current is observed while little current is measured at negative voltages. When the voltage is larger than 1 V, the series resistance dominates and the current increases linearly. The p-type and n-type sections of the nanowire both demonstrate resistive behavior in figure 2(b). The nonlinearity observed in figure 2(b) is attributed to the Schottky barrier at the Ni–Si interfaces [22]. Using the resistances from the I–V curves, along with the nanowire cross sectional area of 1.41×10^{-11} cm^2, the resistivity values of the p-type and n-type sections are calculated to be 0.16 Ω cm and 0.69 Ω cm, respectively. This corresponds to a boron doping concentration of approximately 4×10^{18} cm^{-3} for the p-type section of the nanowire and a phosphorus doping concentration of approximately 6×10^{18} cm^{-3} for the n-type section when estimated using previous results about the relationship between resistivity and doping concentration in polycrystalline silicon [23, 24]. Note that it is hard to precisely estimate the doping concentrations of polycrystalline silicon from resistivity since the resistivity of polycrystalline silicon depends on the grain size and the deposition conditions as well as the doping concentrations [25].

Figure 2(c) shows the ideality factor, η_{ideality}, calculated as [26]:

$$\eta_{\text{ideality}} = \frac{q}{kT}\left(\frac{\mathrm{d}(\ln I)}{\mathrm{d}V}\right)^{-1}, \tag{2}$$

where q is the elementary charge, k is the Boltzmann constant, and T is the absolute temperature. The ideality factor equals to 2 when the recombination current dominates and it equals to 1 when the diffusion current dominates. However, in real devices, the ideality factor can be higher due to the generation and recombination of carriers, the series resistance, the trap-assisted tunneling, and the surface effects [26, 27]. In our p–n junction diode device, the ideality factor is 1.84 at $V = 0.3$ V, but it quickly increases at a higher voltage due to the high series resistance. In addition, since the nanowire is polycrystalline silicon, the higher generation-recombination rates and traps at grain boundaries result in higher ideality factors.

KPFM is a simple and effective tool that allows determination of surface potentials with high spatial resolution [28, 29]. KPFM measures a contact potential difference (CPD) between a conducting AFM tip and a sample which appears owing to the difference in work functions. We used KPFM to characterize the transition region of a laser-direct-written p–n junction nanowire. Figure 3 shows the KPFM CPD profile for a line scan over the transition region along the nanowire. A CPD difference of 110 meV between the p-type and n-type sections of the nanowire is clearly observed. This CPD difference is lower than the theoretical built-in voltage calculated using the following equation [26]:

$$\psi_{\text{bi}} = \frac{kT}{q}\ln\left(\frac{N_{\text{D}}N_{\text{A}}}{n_{\text{i}}^2}\right), \tag{3}$$

where N_{A} is the acceptor impurity concentration, N_{D} is the donor impurity concentration, and n_{i} is the intrinsic carrier concentration. Using the boron concentration of 4×10^{18} cm^{-3} and the phosphorus concentration of 6×10^{18} cm^{-3} which were estimated using the resistivity values of the p–n junction nanowire, the ideal potential difference is ~1.0 V. The discrepancy between the measured CPD and the bulk work function difference in semiconductor materials was previously reported [29–31]. In fact, the measured CPD is related to the surface potential which is different from the work function of the bulk silicon due to the space-charge-layer near the surface [32]. In addition, as our experiments were conducted in air, KPFM is extremely sensitive to surface states due to oxides on the air-exposed area and adsorbates in the air [30, 31]. Therefore, the CPD difference measured across a p–n junction is usually smaller than the bulk built-in potential. For example, CPD differences of 120 meV [29] and 130 meV [33] have been reported between p-type and n-type silicon. In our work, KPFM is mainly used for determining the transition length of the nanowire doping and the transition length of the nanowire doping is about 1.5 μm in figure 3. We believe that the main reason for the broad junction is the finite time period for switching gases during the nanowire deposition. Although the dopant gases were switched within a fraction of a second using computer control, it took a few seconds for the previous dopant gas to

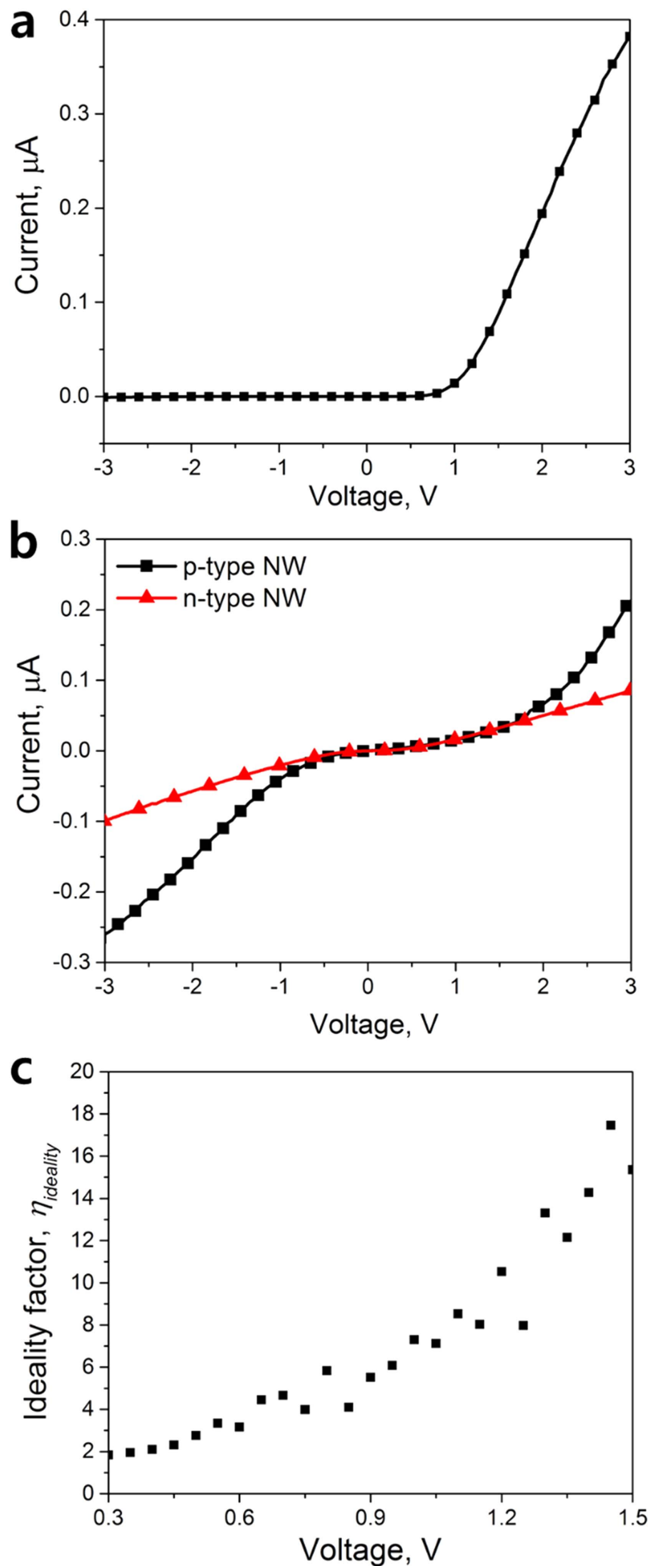

Figure 2. Electrical measurement of the laser-direct-written p–n junction SiNW devices. *I–V* characteristics of (a) p–n junction and (b) p-type (black) and n-type (red) portions of the nanowire. (c) Ideality factor calculated from the *I–V* curve in (a).

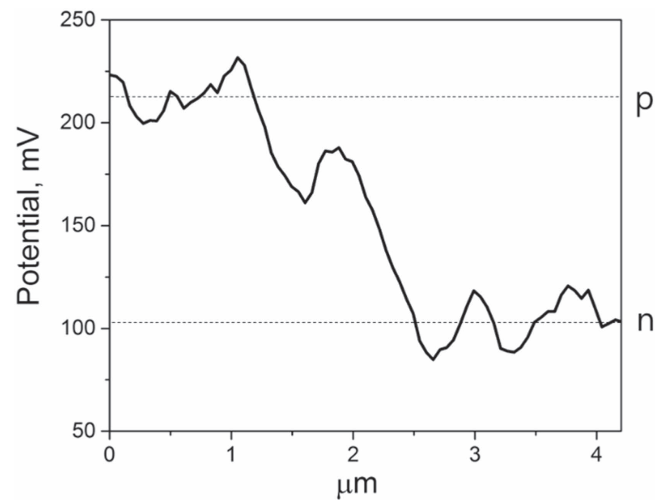

Figure 3. KPFM CPD profile for a line scan over the transition region along a p–n junction nanowire.

be replaced by the new dopant gas in the gas delivery system. Using shorter gas delivery tubing can potential reduce the junction length. On the other hand, the lack of the interference effect in the nanowire longitudinal direction is not believed to be the reason for the broad junction since the nanowire deposition mainly occurs at the tip of the nanowire which is below the diffraction limit due to the lightning rod effect [18].

4. Conclusion

We have demonstrated the capability of the laser-direct-write CVD to synthesize nanowires with dopant modulation that can be used as components for electronic devices. P–n junction nanowires were synthesized by switching dopant gases during nanowire deposition and contacts were fabricated on the nanowires using standard micro-fabrication techniques as a demonstration of device fabrication. Electrical measurements clearly showed the diode behavior of the p–n junction nanowire as well as the resistive behavior of the p-type and n-type sides of the nanowire. KPFM measurement showed the expected modulation in dopant concentration across the p–n transition. We believe that the simplicity and flexibility of our approach could provide a promising alternative for fabrication of many kinds of nanowire devices.

Competing financial interests

The authors declare no competing financial interest.

Acknowledgments

We acknowledge the support of the Defense Advanced Research Projects Agency (Grant No. N66001-08-1-2037) and the National Science Foundation (Grant No. CMMI-1462622).

References

[1] Cui Y and Lieber C M 2001 *Science* **291** 851
[2] Cui Y, Wei Q, Park H and Lieber C M 2001 *Science* **293** 1289
[3] Tutuc E, Appenzeller J, Reuter M C and Guha S 2006 *Nano Lett.* **6** 2070
[4] Tian B, Zheng X, Kempa T J, Fang Y, Yu N, Yu G, Huang J and Lieber C M 2007 *Nature* **449** 885
[5] Vallett A L, Minassian S, Kaszuba P, Datta S, Redwing J M and Mayer T S 2010 *Nano Lett.* **10** 4813
[6] Allen J E *et al* 2008 *Nat. Nanotechnol.* **3** 168
[7] Perea D E, Hemesath E R, Schwalbach E J, Lensch-Falk J L, Voorhees P W and Lauhon L J 2009 *Nat. Nanotechnol.* **4** 315
[8] Imamura G, Kawashima T, Fujii M, Nishimura C, Saitoh T and Hayashi S 2008 *Nano Lett.* **8** 2620
[9] Bäuerle D, Irsigler P, Leyendecker G, Noll H and Wanger D 1982 *Appl. Phys. Lett.* **40** 819
[10] Bernhardt A F, McWilliams B M, Mitlitsky F and Whitehead J C 1986 *Mater. Res. Soc. Symp. Proc.* **75** 633
[11] Bolle M and Lazare S 1993 *J. Appl. Phys.* **73** 3516
[12] Bonse J, Krüger J, Höhm S and Rosenfeld A 2012 *J. Laser Appl.* **24** 042006
[13] Sipe J E, Young J F, Preston J S and van Driel H M 1983 *Phys. Rev.* B **27** 1141
[14] Huang M, Zhao F, Cheng Y, Xu N and Xu Z 2009 *ACS Nano* **3** 4062
[15] Öktem B, Pavlov I, Ilday S, Kalaycıoğlu H, Rybak A, Yavaş S, Erdoğan M and Ilday F Ö 2013 *Nat. Photon.* **7** 897
[16] Halbwax M, Sarnet T, Delaporte P, Sentis M, Etienne H, Torregrosa F, Vervisch V, Perichaud I and Martinuzzi S 2008 *Thin Solid Films* **516** 6791
[17] Vorobyev A Y and Guo C 2008 *Appl. Phys. Lett.* **92** 041914
[18] Mitchell J I, Zhou N, Nam W, Traverso L M and Xu X 2014 *Sci. Rep.* **4** 3908
[19] Xue Z *et al* 2016 *Adv. Funct. Mater.* **26** 5352
[20] Nam W, Mitchell J I, Ye P D and Xu X 2015 *Nanotechnology* **26** 055306
[21] Campbell S A 2008 *Fabrication Engineering at the Micro- and Nanoscale* (New York: Oxford University Press)
[22] Kamins T I, Manoliu J and Tucker R N 1972 *J. Appl. Phys.* **43** 83
[23] Fuhrer M S *et al* 2000 *Science* **288** 494
[24] Seto J Y W 1975 *J. Appl. Phys.* **46** 5247
[25] Briand D, Sarret M, Le Bihan F, Bonnaud O and Pichon L 1995 *Mater. Sci. Technol.* **11** 1207
[26] Colinge J P, Demoulin E, Delannay F, Lobet M and Temerson J M 1981 *J. Electrochem. Soc.* **128** 2009
[27] Sze S M and Ng K K 2007 *Physics of Semiconductor Devices* (Hoboken, NJ: Wiley)
[28] Zhu D, Xu J, Noemaun A N, Kim J K, Schubert E F, Crawford M H and Koleske D D 2009 *Appl. Phys. Lett.* **94** 081113
[29] Koren E, Rosenwaks Y, Allen J E, Hemesath E R and Lauhon L J 2009 *Appl. Phys. Lett.* **95** 092105
[30] Loppacher C, Zerweck U, Teich S, Beyreuther E, Otto T, Grafström S and Eng L M 2005 *Nanotechnology* **16** S1
[31] Robin F, Jacobs H, Homan O, Stemmer A and Bächtold W 2000 *Appl. Phys. Lett.* **76** 2907
[32] Shikler R, Meoded T, Fried N, Mishori B and Rosenwaks Y 1999 *J. Appl. Phys.* **86** 107
[33] Kikukawa A, Hosaka S and Imura R 1995 *Appl. Phys. Lett.* **66** 3510